Significant reduction of vibration and sound in plates at selected modes with combined active and passive damping patches

Joseph Plattenburg[a]
Rajendra Singh[b]
Acoustics and Dynamics Laboratory, Department of Mechanical and Aerospace Engineering
The Ohio State University, Columbus, OH 43210, USA

This paper proposes a refined analytical model, based on the Rayleigh-Ritz method, for vibration of a thin rectangular plate with free boundaries and active and passive damping patches. An acoustic radiation model is also presented which approximates the far-field sound pressure field induced by the plate motion. Case studies of active and passive patches are compared to demonstrate significant vibratory and acoustic attenuation for both broadband and narrowband excitations. A laboratory experiment is used to validate the proposed model, which can be used to determine how patch locations and configurations improve attenuation characteristics. Such a model is of practical importance as structures in a variety of industries (e.g. automotive and aerospace) can be approximated by classical geometries such as thin plates and shells. Compact patches pose a pragmatic solution as they add minimal weight and complexity. Though passive and active methods for noise, vibration, and harshness reduction have heretofore been separately studied, little research has been done on the combined patch approach, in particular with application to acoustic radiation. As such, a computationally-efficient model is still needed to complement large-scale codes for parametric design studies, a method which this paper seeks to provide.

1 INTRODUCTION

Compact damping patches offer potentially attractive solutions to control noise and vibration for a variety of industries, including automotive, aerospace, marine, and appliance, as they add minimal weight and complexity. Significant prior research has been completed on the attenuation characteristics of active patches (such as piezoelectrics), used for both vibration cancelling[1] and shunt damping[2]. Passive constrained layer patches[3,4] have also been used to increase the modal damping of structures. Such studies typically deal with classical geometries[1–7]; however, the effects of concurrent active and passive patches have yet to be studied, particularly for sound radiation from two-dimensional plate geometries using analytical and experimental techniques. As such, the objectives of this paper are as follows. 1) Propose a refined analytical model for vibration and radiated sound from a thin plate with active and/or passive patches. 2) Validate this model with controlled laboratory experiments. 3) Conduct

[a] Email: plattenburg.2@osu.edu
[b] Email: singh.3@osu.edu

illustrative case studies to determine the efficacy of active and/or passive patches for noise and vibration reduction. Some of the mathematical details of the model are formulated by Plattenburg et al.[8], and thus only a condensed version is presented here.

The scope of this work is limited to thin, rectangular, elastic plates with free boundaries. Acoustic radiation will be considered only in the far-field, say from 500 to 1500 Hz. This problem, with the frequency range of interest in particular, stems largely from emerging trends of light-weighting in vehicle industries, which tend to increase vibration and radiated sound. In addition, thin, plate-like vehicle components in hybrid and electric vehicles can be susceptible to sound and vibration in a wider frequency range than with traditional vehicles. Furthermore, in appliance industries, thin sheet metal covers are often used which have vibratory characteristics similar to the plates of this study. Thus, there is a need for improved damping methods—such as compact active or passive patches—as well as enhanced models to predict the sound and vibration response and perform parametric design studies.

2 PROBLEM FORUMULATION FOR PLATE VIBRATION

Consider a thin rectangular plate of dimension $L_x \times L_y$ and thickness h. The plate has free boundaries and is made from a material with Young's modulus E, density ρ, Poisson's ratio ν, and structural damping η. The plate, termed layer 1, may also have a number of active and/or passive damping patches, as shown in Figure 1. Passive patches consist of two layers: a constraining layer (layer 3) and a viscoelastic core (layer 2) with large structural damping. Piezoelectric active patches (layer C) will be assumed to be thin relative to h (thus only negligibly affecting the plate mass and stiffness) and undergo axial extension in the x and/or y directions. The plate may also have an external forcing from a disturbance, F_d, resulting in motion of the base structure as well as a radiated sound pressure field, p.

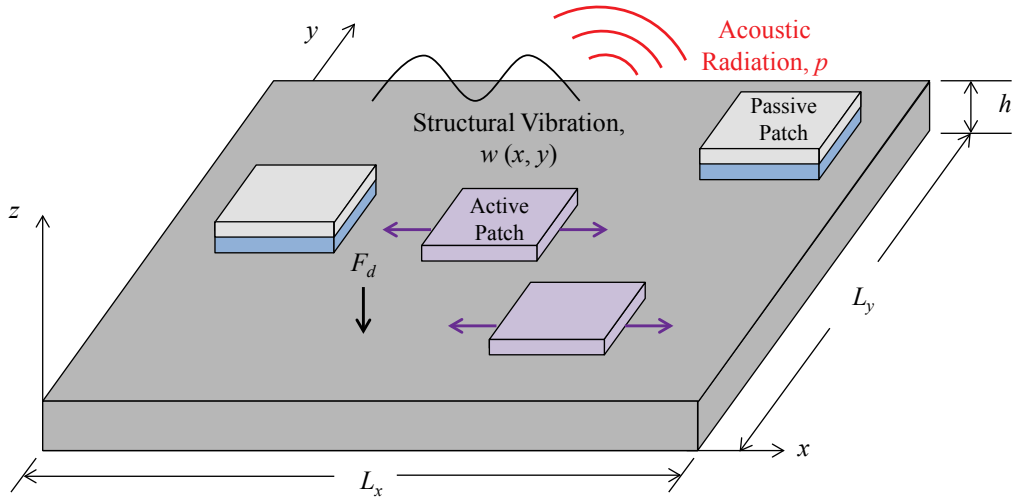

Fig. 1 – Example case: rectangular free plate system with active and passive patches

To quantify the motion of the base structure, the Rayleigh-Ritz method[9] is used. It is assumed that the transverse (z-direction) motion of the base plate, w, is harmonic and written as a linear combination of N assumed shape functions, $\phi\,(x, y)$, with weighting coefficients, q, as:

$$w(x,y;\omega) = e^{j\omega t}\sum_{i=1}^{N} q_i\phi_i(x,y) = e^{j\omega t}\mathbf{q}^{\mathrm{T}}\mathbf{\Phi}(x,y). \tag{1}$$

Here, bold terms denote vectors ($N \times 1$) and pure harmonic response at frequency ω is assumed. The in-plane motions, u and v, as well as shear deformations, γ_x and γ_y, can be similarly expressed for all three layers. Kung and Singh[2] define a minimization scheme that allows all motions for all 3 layers to be expressed in terms of the layer 1 flexural shape function vector, $\mathbf{\Phi}$, reducing the order of the problem to N. The kinetic and potential energy, T_i and U_i, for the i^{th} layer (i = 1, 2, 3) are given by the plate vibration equations from Soedel[10]. Total kinetic and potential energy of the system are obtained in terms of the unknown weighting factors in $\mathbf{q}$ by summing the energies over all three layers and for all passive patches. For a more detailed derivation of these steps, the reader is referred to the literature[2,8].

Non-conservative forcing is introduced to the system by F_d (assumed as a point force) and the input from the active patches, which can be modeled as line moments at the patch boundaries[5]. The generalized forcing vector, $\mathbf{Q}$, is defined as follows, where $F(x, y)$ is the spatial distribution of all non-conservative forces:

$$\mathbf{Q} = \iint_{A_1} F(x,y)\mathbf{\Phi}(x,y)\,dxdy. \tag{2}$$

Lagrange's equation is applied to the energies with respect to the unknown displacement weighting vector $\mathbf{q}$, while maintaining $\mathbf{Q}$ on the right-hand side. The matrix system of equations is then obtained as $\mathbf{M}\ddot{\mathbf{q}} + \mathbf{K}\mathbf{q} = \mathbf{Q}$, where $\mathbf{M}$ and $\mathbf{K}$ are equivalent mass and stiffness matrices[8]. Assuming harmonic excitation and response at ω, the governing equations are written as:

$$\left[\tilde{\mathbf{K}} - \omega^2\mathbf{M}\right]\mathbf{q} = \left\{\tilde{\mathbf{Q}}_d + \tilde{\mathbf{Q}}_c\right\}, \tag{3}$$

where the tilde (~) represents a complex-valued quantity from the loss factor concept, and c and d subscripts refer to the phase-linked active patch control input and the disturbance input F_d, respectively.

3 FORCED HARMONIC RESPONSES AND EXPERIMENTAL VALIDAITION

From the preceding section, Eqn. (3) with $\mathbf{Q}_c = \mathbf{Q}_d = 0$ is used to determine the plate natural frequencies, modal loss factors, and mode shapes. In addition, the harmonic forced response is determined by evaluating $\mathbf{q}$ as a function of frequency and computing the motion, w, from Eqn. (1). Physical dimensions and material properties of the example case, an undamped plate, are given in Table 1 (along with patch properties). Selected natural frequencies, along with corresponding modal indices of the undamped system, are summarized in Table 2. A comparison with the commercial finite element software, Abaqus[11], shows good agreement.

Table 1 – Material properties for a rectangular plate and patches

Layer	Material	Young's Modulus	Density [kg-m^{-3}]	Poisson's Ratio	Thickness [mm]	Loss Factor	Area ($L_x \times L_y$) [mm]
1	Aluminum	63 GPa	2606	0.33	3.2	0.0013	277 × 174
2	Adhesive	6.2 MPa	730	0.40	0.94	1.25	76.2 × 25.4
3	Steel	203 GPa	7600	0.30	0.38	0.005	76.2 × 25.4
C	Composite	31 GPa	-	0.35	0.3	-	28.3 × 16.0

Table 2 – Selected natural frequencies of the undamped plate from Table 1

Mode	Modal Index	Natural Frequency [Hz]		
		Analytical	FEM*	Experimental
1	(1, 1)	210	204	203
2	(2, 0)	223	211	210
3	(2, 1)	483	466	468
4	(0, 2)	566	554	552
6	(1, 2)	710	703	709
8	(2, 2)	1061	1026	1023
9	(4, 0)	1206	1192	1193

*Finite Element Method: Abaqus with shell elements

Modal indices, (m, n), are the number of nodal lines parallel to the y and x axes, respectively. The displacement shape of the (4, 0) mode is shown in Figure 2a. The cross-point accelerance spectrum (defined as acceleration per unit input force), G_{af}, at measurement location $(\overline{x}_0, \overline{y}_0) = (0.025, 0.025)$ due to forcing at $(\overline{x}_d, \overline{y}_d) = (0.45, 0.45)$ is plotted in Figure 2b. Here, over-bars indicate locations normalized by plate length (i.e. $\overline{x} = x/L_x$). The peaks in the spectrum are seen to correlate with the expected natural frequencies from Table 2. The (4, 0) mode, shown in Figure 2a and circled in the magnitude spectrum of Figure 2b, will be considered as the primary mode of interest for this study, as it is within the desired frequency range, has low modal damping, and is well isolated.

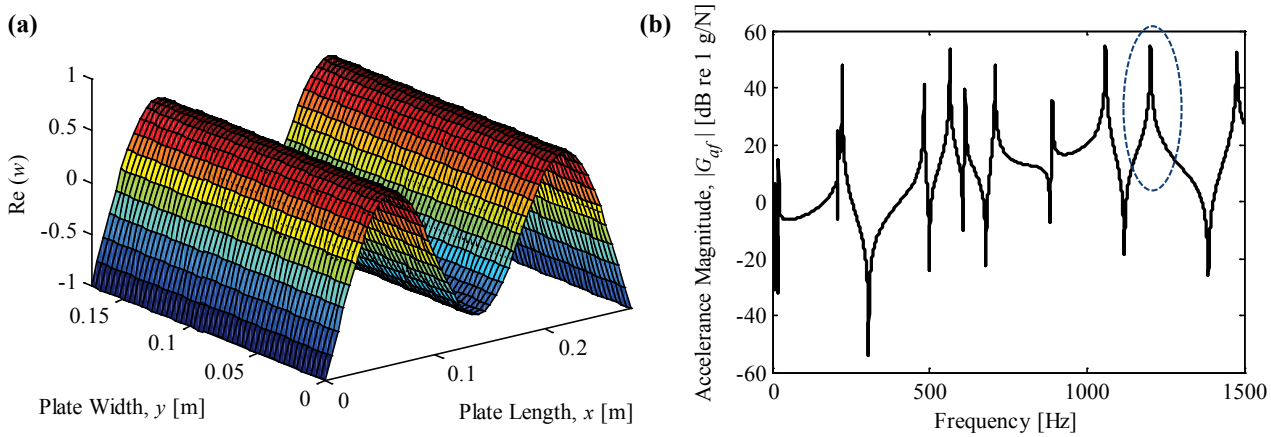

Fig. 2 – Vibration predictions: (a) displacement shape of the (4, 0) mode; (b) cross-point accelerance spectrum with the (4, 0) mode indicated

The proposed model has been validated extensively in terms of vibration[8], and a subset of those experimental results is presented here. An impact hammer test is used to determine the undamped natural frequencies, and the results in Table 2 show good correlation with theory and FEM. The hammer is also used to excite the plate with a single damping patch (located to target the (2, 2) and (4, 0) modes), and the cross point accelerance is measured. This measurement, along with the corresponding analytical prediction, is shown in Figure 3a, where good agreement is seen. Modal loss factors are estimated using a least squares algorithm and compared with the analytical prediction for a different patch configuration (to target the (4, 0) mode but not the (2, 2) mode) in Figure 3b. Again, good agreement is observed. Additional validation studies, in terms of vibration response with an active patch, are reported in a prior paper[8].

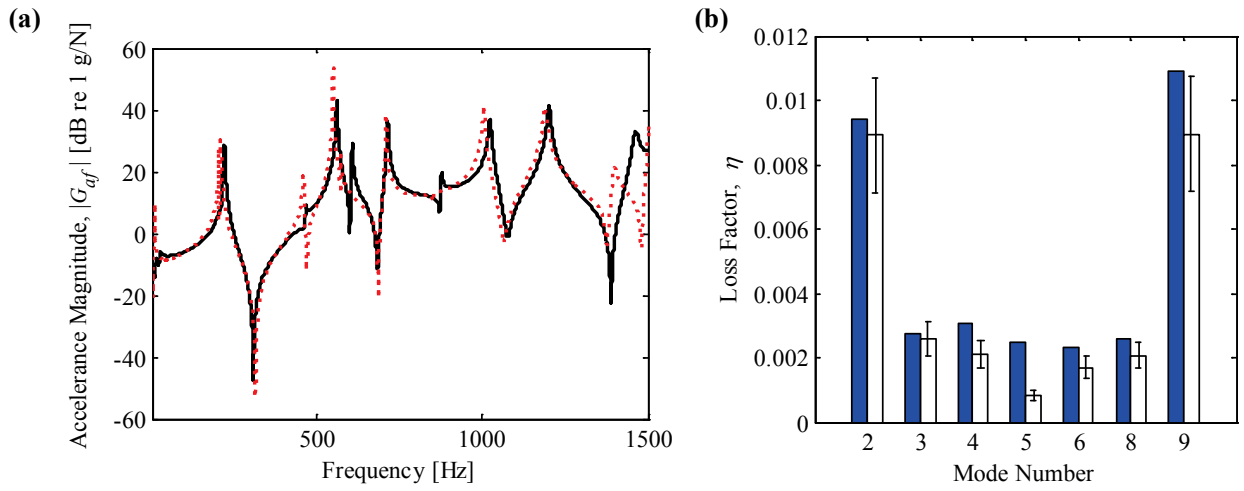

Fig 3 – Experimental validation of theory for passive patches: (a) accelerance magnitude spectra, prediction (—) and measurement (···); (b) modal loss factors, prediction (■) and measurement (□) with error bars

4 ACOUSTIC RADIATION MODEL AND EXPERIMENTAL VALIDATION

A far-field acoustic radiation model, using the Rayleigh integral approximation[12], is presented here. The plate is assumed to be surrounded by an infinite baffle in the plane $z = 0$, and radiates sound into the semi-infinite $+z$ space due to the transverse motion—$w(x, y)$ from Eqn. (1). The harmonic acoustic pressure amplitude in Cartesian coordinates, $p(x', y', z')$, where the (x', y', z') coordinate system has its origin at the center of the plate, is given in the far field by[12]:

$$p(x', y', z'; \omega) = \rho_a \omega^2 \int_0^{L_x} \int_0^{L_y} w(x, y) \frac{e^{-jkr}}{2\pi r} dxdy \tag{4a}$$

$$r^2 = \left(x' - x + \frac{L_x}{2} \right)^2 + \left(y' - y + \frac{L_y}{2} \right)^2 + (z')^2 . \tag{4b}$$

Here, ρ_a is the acoustic fluid density, $k = \omega/c_o$ is the acoustic wavenumber where c_o is the speed of sound in the acoustic fluid (here, air), and r is the distance from a given point on the plate (x, y, $z = 0$) to an observer in the semi-infinite space, (x', y', $z' > 0$). Sound pressure level (SPL), L_p, is defined as follows, where p_{rms} is the RMS value of p and p_{ref} is the reference pressure, 20 μPa:

$$L_p [dB] = 10 \log_{10} \left(\frac{p_{rms}^2}{p_{ref}^2} \right) = 20 \log_{10} \left(\frac{p_{rms}}{p_{ref}} \right). \tag{5}$$

Analyses will be performed at harmonic frequency from 500 to 1500 Hz and at the mode of interest, for which the frequency ω is determined from Table 2 as ω_n [rad/s] = $2\pi f_n$ [Hz]. To ensure that measurements are made in the far-field (regime of validity for Eq. 4), we must satisfy $kr >> 1$. Beyond 500 Hz and at measurement distance $r \approx 0.5$ m, $kr \geq 5$ is sufficient for the far-field approximation. A single spatial location above the plate ($x' = 0$, $y' = 0$) is used for measurement. While the effect of patches on the spatial variation of p is outside the scope of this paper, this concept may be studied in the future.

An analogous experiment is designed and built for validation of the acoustic model. The experiment consists of placing the plate (with free boundaries and no baffle) from Figure 1 (with excitation from an electrodynamic shaker) in an anechoic chamber where both acoustic and vibratory measurements can be made. A schematic of this experiment is shown in Figure 4.

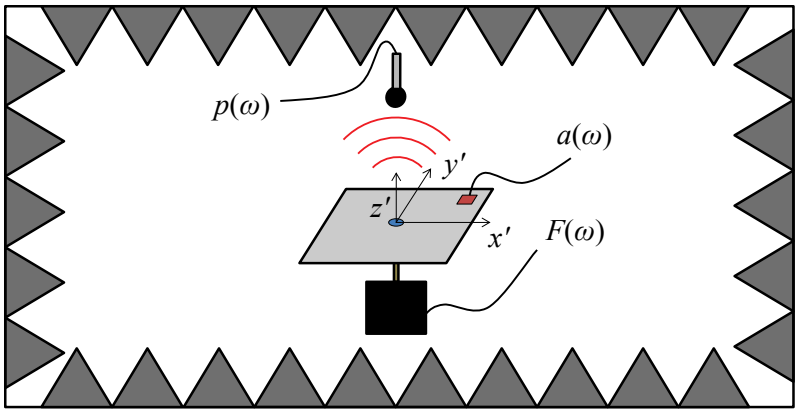

Fig. 4 – Vibro-acoustic experiment with shaker excitation in anechoic chamber

Using Eqn. (4a), the acoustic sensitivity spectrum, G_{pf} (defined as pressure per input force) is written as:

$$\tilde{G}_{pf}(\omega) = \tilde{p}(\omega) / \tilde{F}(\omega). \tag{6}$$

This transfer function is predicted at (x', y', z') = (0, 0, 0.5 m) and its magnitude is plotted in Figure 5a (solid black line). Here, high sound pressure levels are seen corresponding to the resonant modes (in particular, the (0, 2), (2, 2) and (4, 0) modes). Away from resonance, the sound pressure is relatively uniform, consistent with "below-coincidence frequency" response. A corresponding experiment is performed by measuring the acoustic sensitivity spectrum due to the point-like excitation force from a shaker at the same (x', y', z') location, and the measurements are given in Figure 5b (again, solid black line). Away from resonances, relatively uniform sound pressure is seen, and at resonances G_{pf} is significantly increased. Overall, relatively good correlation is seen between experiment and the model in the frequency range of interest.

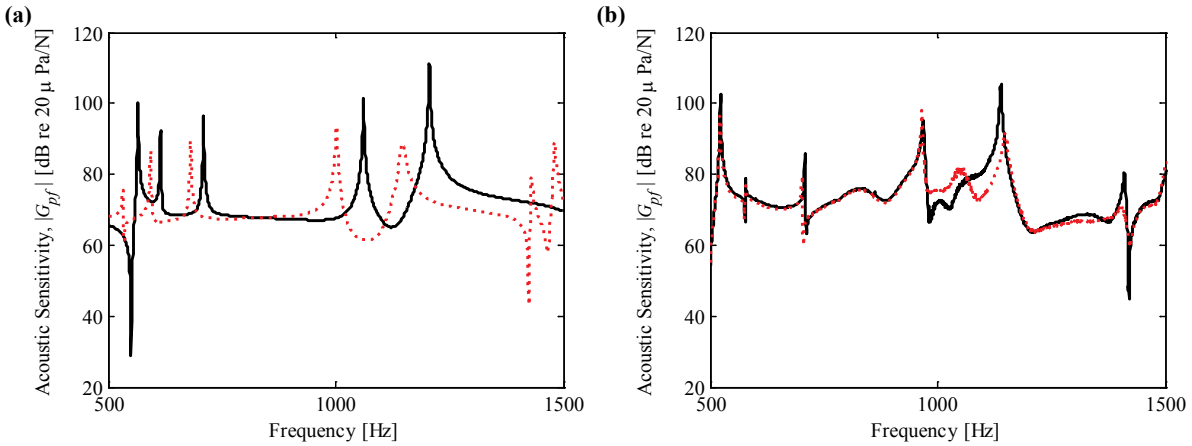

Fig. 5 – Radiated sound pressure spectra (normalized by input force), undamped plate (—), and plate with passive damping patch (···): (a) prediction; (b) measurement

5 CASE STUDIES FOR ACTIVE AND PASSIVE PATCHES

For Case 1, a passive patch is applied to the structure to increase modal damping. Next, for Case 2, an active patch is used to enact active control by cancelling out radiated sound (near the (4, 0) mode) at a measurement location induced by a disturbance. The patch locations for the two cases, along with force input location and acceleration measurement location, are shown in Figure 6.

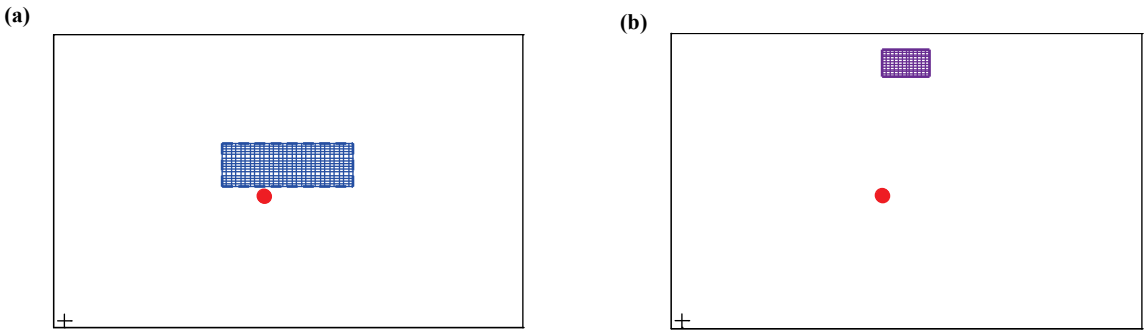

Fig. 6 – Patch locations, with passive patch (■), active patch (■), force location (●) and acceleration measurement location (+): (a) Case 1; (b) Case 2

For the first case, a harmonic force input is assumed (up to 1500 Hz) and the acoustic sensitivity G_{pf} is determined. The results from the model are shown in Figure 5a. Here significant insertion loss (*IL*), relative to the undamped case, of the (4, 0) mode is observed (~22 dB), while less reduction is seen at the (2, 2) mode. Insertion loss is defined as the difference in SPL between the treated and baseline (virtually undamped plate) cases:

$$IL = 20\log 10\left(\frac{p_{rms,baseline}}{p_{rms,treated}}\right) = L_{p,baseline} - L_{p,treated}. \tag{7}$$

The corresponding experiment (Figure 5b) yields similar results with no attenuation at the (2, 2) mode and significant damping of the (4, 0) mode. The measured *IL* at the (4, 0) mode is around 13 dB in this case, though it should be noted that in the "undamped" case, the accelerometer on the plate added additional damping and mass loading. As such, it would be expected that the model would over-predict the attenuation relative to the experiment. Nevertheless, the model shows good agreement with the trends observed experimentally, in particular significant attenuation of the mode of interest.

For Case 2 of Figure 6, the force excitation is assumed as a narrowband sinusoidal signal near the (4, 0) natural frequency. Here the control input to the active patch is chosen such that *p* (induced by the active patch) at the acoustic field measurement location is equal in magnitude, but out of phase from *p* induced by the disturbance force (0.063 N_{peak} at 1206 Hz). The relative phase between the control input and force is swept from −180° to 180° for reference. The resulting radiated sound pressure as predicted by the model is shown in Figure 7a. Observe that the control and disturbance amplitudes are equal and at an "optimal" phase angle (here around 180°), the radiated sound pressure is reduced by nearly 40 dB. At an angle of 180° opposite the optimal value, the amplitude is increased by 6 dB. A corresponding experiment (with excitation at 1135 Hz) again yields similar results, shown in Figure 7b.

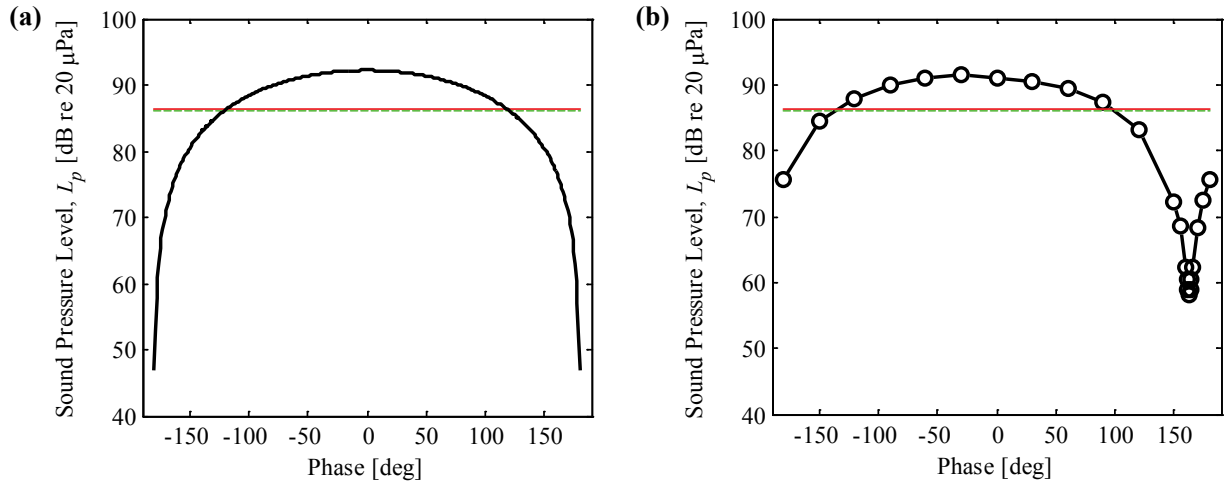

Fig. 7 – Active control of sound pressure level at (4, 0) mode as a function of control phase, with response from force (—) and from control (- - -): (a) prediction of controlled SPL (—); (b) measurement of controlled SPL (-○-)

At the optimal phase, *IL* of nearly 30 dB is seen; note that this value is highly dependent on very precise control parameters, the fidelity of the measurement system, and the noise floor amplitude. The optimal phase here is seen to be around 165°, rather than 180° due to the dynamics of the shaker and the active patch (i.e. phase lag induced by capacitance, etc.). Overall, the agreement between the model and experiment is good, showing significant reduction of the sound pressure level.

6 CONCLUSION

This paper presents a refined model for the vibration and radiated sound of a thin plate with compact active and passive damping patches. The model is validated with laboratory experiments in terms of the natural frequencies, modal damping ratios, and forced response. The acoustic radiation from the frequency range of interest is also validated with microphone measurements at a selected location, where good agreement is seen. Two case studies are then investigated using a passive damping patch as well as active control with an active patch. Both methods are found to result in significant attenuation of sound pressure at a targeted mode, as summarized in Table 3. Approximate vibratory *IL* results from a prior paper[8] are also included for the sake of comparison. It should be noted that all *IL* measurements should be considered ±2 dB due to measurement uncertainty and simplifying assumptions in the model. The proposed analytical model gives reasonable predictions in terms of the vibration and radiated sound pressure for the undamped case as well as with active and passive patches, and shows some of the benefits of using active noise and vibration control.

Table 3 – Acoustic and vibration insertion losses for two cases at the (4, 0) mode

	Acoustic *IL* [dB]		Vibration *IL*[8] [dB]	
	Predicted	Measured	Predicted	Measured
Case 1 (Passive Patch)	22	13	14	14
Case 2 (Active Patch)	39	28	42	49
Improvement over Passive	*17*	*15*	*28*	*35*

In a recent work[8], the effect of combining active and passive patches for vibration control is investigated, where a complicated interaction involving the control phase is found. While the current research is still in progress, future studies are expected to extend the acoustic model proposed here to the combined active and passive patch case. This study would be of particular importance, as the acoustic radiation problem involves complicated phase effects to begin with, and comprehensive models, as proposed here, would be needed to address the additional complications induced by active and passive patches. Overall, the simplified models presented in this paper provide valuable insight into the acoustic radiation problem. This method should allow rapid analysis and parametric design studies in terms of active and passive patches for the many structures in industry that may be approximated as thin plates with classical boundary conditions and well defined mode shapes.

ACKNOWLEDGEMENTS

The authors would like to acknowledge the OSU Graduate School, the Ohio Space Grant Consortium, the Smart Vehicle Concepts Center (www.SmartVehicleCenter.org), and the National Science Foundation Industry/University Cooperative Research Centers program (www.nsf.gov/eng/iip/iucrc) for funding this work through graduate fellowships and financial assistance.

REFERENCES

1. E. K. Dimitriadis, C. R. Fuller, and C. A. Rogers, Piezoelectric Actuators for Distributed Vibration Excitation of Thin Plates, *Journal of Vib. and Acoustics*, 113 (1991) 100–107.
2. J. Hosberg and A. Le Coent, Explicit Solution Format for Complex-Valued Natural Frequency of Beam with R-Shunted Piezoelectric Laminate Transducer, *Proc. IMechE Part C: Journal of Mechanical Engineering Science*, 228 (1) (2013), 31–44.
3. S. W. Kung and R. Singh, Complex Eigensolutions of Rectangular Plates with Damping Patches, *Journal of Sound and Vibration*, 216 (1) (1998) 1–28.
4. S. W. Kung and R. Singh, Vibration Analysis of Beams with Multiple Constrained Layer Damping Patches, *Journal of Sound and Vibration*, 212 (5) (1998) 781–805.
5. E. F. Crawley and J. de Luis, Use of Piezoelectric Actuators as Elements of Intelligent Structures, *AIAA Journal*, 25 (10) (1987) 1373–1385.
6. H. Zheng, C. Cai, G. S. H. Pau, G. R. Liu, Minimizing Vibration Response of Cylindrical Shells through Layout Optimization of Passive Constrained Layer Damping, *Journal of Sound and Vibration*, 279 (2005) 739–756.
7. V. R. Sonti and J. D. Jones, Curved Piezoactuator Model for Active Vibration Control of Cylindrical Shells, *AIAA Journal*, 34 (5) (1996) 1034–1040.
8. J. Plattenburg, J. T. Dreyer, and R. Singh, Active and Passive Patches on a Thin Rectangular Plate: A Refined Analytical Model with Experimental Validation, in press, *Journal of Sound and Vibration*, 2015.
9. L. Meirovitch, *Fundamentals of Vibrations*, McGraw-Hill, New York, 2001.
10. W. Soedel, *Vibrations of Plates and Shells*, Marcel Dekker, New York, 2004.
11. Abaqus Finite Element Analysis, Ver. 6.13, <http://www.3ds.com/products-services/simulia/portfolio/abaqus/>, accessed Oct. 28, 2014.
12. E. G. Williams and J. D. Maynard, Numerical Evaluation of the Rayleigh Integral for Planar Radiators using the FFT, *Journal of the Acoustical Society of America*, 72 (6) (1982), 2020–2030.